Operator analysis of effective spin-flavor interactions for $L = 1$ excited baryons

Cintia Willemyns and Carlos Schat

Departamento de Física, FCEyN, Universidad de Buenos Aires and IFIBA, CONICET,
Ciudad Universitaria, Pabellón 1, 1428 Buenos Aires, Argentina
(Received 12 November 2015; published 5 February 2016)

We match the nonrelativistic quark model, with both flavor-dependent and flavor-independent effective quark-quark interactions, to the spin-flavor operator basis of the $1/N_c$ expansion for the $L = 1$ nonstrange baryons. We obtain analytic expressions for the coefficients of the $1/N_c$ operators in terms of radial integrals that depend on the shape and relative strength of the spin-spin, spin-orbit and tensor interactions of the model, which are left unspecified. We obtain several new, parameter-free relations between the seven masses and the two mixing angles that can discriminate between different spin-flavor structures of the effective quark-quark interaction. We discuss in detail how a general parametrization of the mass matrix depends on the mixing angles and is constrained by the assumptions on the effective quark-quark interaction. We find that, within the present experimental uncertainties, consistency with the best values of the mixing angles as determined by a recent global fit to masses and decays does not exclude any of the two most extreme possibilities of flavor-dependent (-independent) quark-quark interactions, as generated by meson (gluon) exchange interactions.

I. INTRODUCTION

In the last 15 years a large amount of data on electroproduction of mesons was accumulated at different facilities, with the purpose of determining the resonance contribution to the cross sections and identifying the members of the excited baryon spectrum. The goal is to obtain a precise description of the first excited states of the ground-state baryons, which is an important test for our understanding of QCD in the low-energy, strong-coupling regime. Models try to capture the most relevant physics giving a description in terms of effective degrees of freedom, but it is hard to make an estimate of the theoretical errors involved and there is little guide on how to improve on them. On the other hand, lattice calculations are based on first principles and recently they have shown a significant progress in the determination of the light baryon mass spectrum and the identification of the spin-parity of the excited states [1,2]. The lattice results seem to confirm the old quark model picture, where the light-flavored baryons fill irreducible representations of the orbital × spin-flavor group $O(3) \times SU(6)$. Empirically there are still many missing states in the spin-flavor multiplets of the quark model, an old problem that has constantly spurred the experimental program in the search of new resonances. For recent reviews on the experimental status of excited baryons and quark-model-related discussions see Refs. [3–5].

An alternative approach to study the phenomenology of baryons is to consider the large-N_c limit of QCD [6,7], where it has been shown that the spin-flavor symmetry for baryons arises from consistency relations for pion-nucleon scattering [8–12]. The predictions of this symmetry for the masses and the couplings explain some of the successes of the nonrelativistic quark model [13]. The breaking of the spin-flavor symmetry can be studied systematically in a $1/N_c$ expansion using quark operators, establishing a deep connection between QCD and the quark model [14–16].

The $1/N_c$ expansion was first applied to the masses and axial couplings of ground-state baryons [13–16] and later to study the masses of the negative-parity $L = 1$ excited baryons [17–22] with great success. The strong and electromagnetic properties of these states, as well as of resonances in other spin-flavor multiplets have also been studied in the $1/N_c$ expansion and a number of interesting results were obtained; see Ref. [23] for a review, and references therein.

Recently, the $1/N_c$ expansion has also been put in connection with the lattice calculations of the baryon spectrum [24–26] discussing the spin-flavor composition of the baryons and the quark mass dependence of the results. However, in the systematic operator expansion provided by the $1/N_c$ approach, all the nonperturbative dynamics remains hidden in the values of the operator coefficients that in a phenomenological analysis have to be fitted to data. The physics driving the relative numerical sizes of operator coefficients remains unknown. Comparison with the results of lattice calculations give some insight on their quark mass dependence but an interpretation in terms of effective degrees of freedom and their interactions is missing.

It is therefore very desirable to put the $1/N_c$ expansion in closer connection with dynamical calculations, such as the one provided by the quark model, in order to arrive at a

034007-1

simple physical picture in terms of effective degrees of freedom. As a first step toward this goal, a very general method to match quark model interactions to the $1/N_c$ operators was presented in Ref. [27] using the permutation group S_N, for arbitrary N_c, generalizing a similar analysis for $N_c = 3$ done by Collins and Georgi in Ref. [28]. As an application, the most general two-body interaction excluding three-body forces was considered in Ref. [29] without making any assumptions on the form of the confining potential, obtaining as a result Eq. (5) in Ref. [29], shown again as Eq. (34) below, which gives a correlation between the mixing angles of the $L = 1$ nonstrange excited baryons.

In Ref. [30], a particular version of the quark model (QM) containing only spin-spin and quadrupole flavor-independent interactions, the Isgur-Karl (IK) model [31,32], has been matched to the $1/N_c$ operator expansion. Due to the harmonic oscillator confining potential adopted in this model, the wave functions can be found exactly, and the center-of-mass motion can be taken into account explicitly. This analysis was extended in Ref. [33] by keeping only the spin-spin interaction but allowing for the most general flavor dependence of the quark-quark interaction, neglecting the quadrupole and spin-orbit interaction. In the present work we consider the most general quark-quark spin-flavor interaction, taking into account all three components of the interaction, and allowing for the most general spin-flavor structure.

We focus here on the mass spectrum of the lightest $L = 1$ baryons, the nonstrange members of the negative-parity SU(6) **70**-plet. Configuration mixing is neglected as has been done in previous $1/N_c$ analysis, noting that this mixing is driven by the numerically suppressed spin-orbit operators [26].

The general spin-flavor structure of the interactions can be reduced to two extreme cases, where we only have flavor-independent interactions as obtained in model interactions based on one-gluon exchange (OGE), or flavor-dependent interactions that arise in model interactions based on one-meson exchange (OME). Considering different spin-flavor structures for the interaction we obtain several new mass-angle relations that are parameter free. Even in the most general case they are sufficient to constrain the mixing angles. They will be shown to be compatible with the latest determination of the angles from a global fit to the masses, decay widths and photocouplings [34]. The operator coefficients of the best fit are also compared with our fits and nontrivial correlations among the coefficients that connect them with the details of the microscopic quark-quark interaction are uncovered.

The paper is organized as follows. In Sec. II we present the physical states and define the mixing angles. In Sec. III we present the model interactions. In Sec. IV we present the general parametrization of the mass matrix. In Sec. V we present the mass-angle relations for the general case and for the more restrictive OGE and OME model interactions.

In Sec. VI we discuss the fits and in Sec. VII we discuss the connection with the $1/N_c$ operators. In Sec. VIII we present our conclusions. In Appendix A we list the $1/N_c$ operators. Useful expressions for the general form of the mass matrix and its relation to the mixing angles are given in Appendix B. In Appendix C we show the linear dependences among operators relevant for $N_c = 3$. The detailed analytic expressions that connect our results with the $1/N_c$ studies are presented in Appendix D. In Appendix E we give the explicit expressions of the coefficients as a function of the angles. In Appendix F we cross-check our general expressions and show how they reduce in the simplest version of the QM, the IK model.

II. QUARK MODEL AND PHYSICAL STATES

We consider a nonrelativistic quark model for baryons, described by the Hamiltonian H_0 for three quarks of constituent mass m with two-body harmonic interactions

$$H_0 = \frac{1}{2m} \sum_i p_i^2 + \frac{K}{2} \sum_{i<j} r_{ij}^2, \qquad (1)$$

where K is a model parameter. This Hamiltonian can be diagonalized exactly and the center-of-mass (c.m.) motion decouples when H_0 is expressed in terms of the relative coordinates $\vec{\rho} = \frac{1}{\sqrt{2}}(\vec{r}_1 - \vec{r}_2)$ and $\vec{\lambda} = \frac{1}{\sqrt{6}}(\vec{r}_1 + \vec{r}_2 - 2\vec{r}_3)$. The Hamiltonian takes the form of two independent oscillators

$$H_0 = \frac{p_\rho^2}{2m} + \frac{p_\lambda^2}{2m} + \frac{3}{2}K\rho^2 + \frac{3}{2}K\lambda^2, \qquad (2)$$

where $\vec{p}_\rho = -i\partial/\partial\vec{\rho}$, $\vec{p}_\lambda = -i\partial/\partial\vec{\lambda}$.

Here we will consider the first excited states carrying one unit of angular momentum, which correspond to the lowest-energy negative-parity baryons that belong to the mixed symmetric (MS) $\mathbf{20_{MS}}$ multiplet of spin-isospin $SU(4)$. The eigenstates $\Psi_{Lm}^{\rho,\lambda}$ of H_0 with $L = 1$, $m = 1$ are

$$\Psi_{11}^\rho = \rho_+ \frac{\alpha^4}{\pi^{3/2}} \exp\left(-\frac{1}{2}\alpha^2(\rho^2 + \lambda^2)\right), \qquad (3)$$

$$\Psi_{11}^\lambda = \lambda_+ \frac{\alpha^4}{\pi^{3/2}} \exp\left(-\frac{1}{2}\alpha^2(\rho^2 + \lambda^2)\right), \qquad (4)$$

where $\alpha = (3Km)^{1/4}$, $\rho_+ = \rho_x + i\rho_y$, $\lambda_+ = \lambda_x + i\lambda_y$ and the combination $\rho^2 + \lambda^2$ is invariant under permutations of the three quarks.

The quark spin of the MS $I = 1/2$ states takes the values $S = 1/2$, $3/2$, which combined with the orbital angular momentum $L = 1$ gives the following N states: two states with $J = 1/2$ denoted $^2N_{1/2}$, $^4N_{1/2}$, two states $J = 3/2$ denoted $^2N_{3/2}$, $^4N_{3/2}$, and one state with $J = 5/2$ denoted

$^4N_{5/2}$. In addition, there are also spin-isospin MS $I = 3/2$ states with $S = 1/2$, which result in two $J = 1/2, 3/2$ states, denoted as $^2\Delta_{1/2}, ^2\Delta_{3/2}$.

The MS spin-isospin states are coupled with the MS spatial states given in Eqs. (3) and (4) to form completely

symmetric states with the right quantum numbers, anti-symmetrized by the color-singlet wave function, which factorizes from all our calculations and can be omitted. Explicitly the MS quark model states $^{2S+1}N_J$ and $^{2S+1}\Delta_J$ are given by

$$|^2N_J; J_3 I_3\rangle = \frac{1}{2} \sum_{m,S_3} \begin{pmatrix} 1 & \frac{1}{2} & | & J \\ m & S_3 & | & J_3 \end{pmatrix} [(\xi^\rho_{S_3}\varphi^\rho_{I_3} - \xi^\lambda_{S_3}\varphi^\lambda_{I_3})\Psi^\lambda_{1m} + (\xi^\rho_{S_3}\varphi^\lambda_{I_3} - \xi^\lambda_{S_3}\varphi^\rho_{I_3})\Psi^\rho_{1m}], \tag{5}$$

$$|^4N_J; J_3 I_3\rangle = \frac{1}{\sqrt{2}} \sum_{m,S_3} \begin{pmatrix} 1 & \frac{3}{2} & | & J \\ m & S_3 & | & J_3 \end{pmatrix} \xi^{3/2}_{S_3}(\varphi^\rho_{I_3}\Psi^\rho_{1m} + \varphi^\lambda_{I_3}\Psi^\lambda_{1m}), \tag{6}$$

$$|^2\Delta_J; J_3 I_3\rangle = \frac{1}{\sqrt{2}} \varphi^{3/2}_{I_3} \sum_{m,S_3} \begin{pmatrix} 1 & \frac{1}{2} & | & J \\ m & S_3 & | & J_3 \end{pmatrix} (\xi^\rho_{S_3}\Psi^\rho_{1m} + \xi^\lambda_{S_3}\Psi^\lambda_{1m}), \tag{7}$$

where φ and ξ are isospin and spin states that are orthonormal. The explicit spin states relevant for the calculation are

$$\xi^{3/2}_{3/2} = |\uparrow\uparrow\uparrow\rangle, \tag{8}$$

$$\xi^\rho_{1/2} = \frac{1}{\sqrt{2}}(|\uparrow\downarrow\uparrow\rangle - |\downarrow\uparrow\uparrow\rangle), \tag{9}$$

$$\xi^\lambda_{1/2} = -\frac{1}{\sqrt{6}}(|\uparrow\downarrow\uparrow\rangle + |\downarrow\uparrow\uparrow\rangle - 2|\uparrow\uparrow\downarrow\rangle), \tag{10}$$

where the other spin projections can be obtained by applying the lowering operator, and similarly for isospin.

The physical states of angular momentum J are a mixture of quark model states, as the quark spin S is not a good quantum number. The mixing angles are defined as

$$N_{J=1/2}(1535) = \cos\theta_1 {}^2N_{1/2} + \sin\theta_1 {}^4N_{1/2},$$
$$N'_{J=1/2}(1650) = -\sin\theta_1 {}^2N_{1/2} + \cos\theta_1 {}^4N_{1/2}, \tag{11}$$

for the $J = 1/2$ nucleons, and

$$N_{J=3/2}(1520) = \cos\theta_3 {}^2N_{3/2} + \sin\theta_3 {}^4N_{3/2},$$
$$N'_{J=3/2}(1700) = -\sin\theta_3 {}^2N_{3/2} + \cos\theta_3 {}^4N_{3/2}, \tag{12}$$

for the $J = 3/2$ nucleons [35]. It is always possible to bring the mixing angles into the range $[-\pi/2, \pi/2]$ by appropriate phase redefinitions of the physical states, and this is the definition we will use throughout this paper.

III. MODEL INTERACTIONS AND THEIR SPIN-FLAVOR STRUCTURE

The spin-isospin symmetric Hamiltonian H_0 contributes an average mass m_0 to all members of an $SU(4) \times O(3)$ multiplet. In order to describe the mass splittings of the negative-parity baryons we will add to H_0 the spin-isospin-dependent two-body interaction terms V_{ij}

$$H = H_0 + \sum_{i<j} V_{ij} = H_0 + V_{ss} + V_{so} + V_t, \tag{13}$$

which are labeled according to their transformation properties under orbital angular momentum ℓ: the $\ell = 0$ spin-spin interaction V_{ss}, the $\ell = 1$ spin-orbit interaction V_{so} and the $\ell = 2$ quadrupole interaction V_t. We write these interaction terms in a generic form, leaving their radial dependence unspecified, following Refs. [27,28] as

$$V_{ss} = V^0_{ss} + V^1_{ss} = \sum_{i<j=1}^3 v_{ss}(r_{ij})\vec{s}_i \cdot \vec{s}_j, \tag{14}$$

$$V_{so} = V^0_{so} + V^1_{so}$$
$$= \sum_{i<j=1}^3 v_{so}(r_{ij})[(\vec{r}_{ij} \times \vec{p}_i) \cdot \vec{s}_i - (\vec{r}_{ij} \times \vec{p}_j) \cdot \vec{s}_j$$
$$+ 2(\vec{r}_{ij} \times \vec{p}_i) \cdot \vec{s}_j - 2(\vec{r}_{ij} \times \vec{p}_j) \cdot \vec{s}_i], \tag{15}$$

$$V_t = V^0_t + V^1_t = \sum_{i<j=1}^3 v_t(r_{ij})[3(\hat{r}_{ij} \cdot \vec{s}_i)(\hat{r}_{ij} \cdot \vec{s}_j) - (\vec{s}_i \cdot \vec{s}_j)], \tag{16}$$

with $v_\varkappa(r_{ij}) = v^0_\varkappa(r_{ij}) + v^1_\varkappa(r_{ij})\tau^a_i\tau^a_j$, where $\varkappa = ss, so, t$, labels the $v^{0,1}_\varkappa$ radial functions that we take as unknown. The superscript 0 (1) indicates the absence (presence) of the isospin-dependent $\tau_i \cdot \tau_j$ interactions. Setting $v^1_\varkappa = 0$

($v_\varkappa^0 = 0$) we obtain the isospin-independent (-dependent) interactions that we label as OGE (OME), respectively, as they can be typically obtained starting from one-gluon exchange [36] or one-meson exchange [37,38] model interactions. We label the general quark model as defined by Eqs. (13)–(16) as the OGE + OME quark model.

As is well known [32], although we start from two-body interactions, it is remarkable that after removing the c.m. motion the spin-orbit potential develops a three-body interaction, as can be seen from its $(ij) = (12)$ component

$$(V_{so})_{12} = 3v_{so}(\sqrt{2}\rho)\left[(\vec{\rho} \times \vec{p}_\rho) \cdot (\vec{s}_1 + \vec{s}_2)\right.$$
$$\left. - \frac{1}{3\sqrt{3}}(\vec{\rho} \times \vec{p}_\lambda) \cdot (\vec{s}_1 - \vec{s}_2)\right]$$
$$\equiv (V_{so-2B})_{12} + (V_{so-3B})_{12}, \qquad (17)$$

where the two-body component V_{so-2B} and the three-body component V_{so-3B} are defined by the first and second term, respectively.

IV. MASS MATRIX PARAMETRIZATION AND OPERATOR MATCHING

Here we present the general structure we obtain for the mass matrix of the $[\mathbf{20_{MS}}, 1^-]$ nonstrange excited baryons starting from the generic quark model defined by Eqs. (13)–(16). We also discuss the matching to the effective spin-flavor operators that appear in the studies of excited baryons using

the $1/N_c$ expansion, as defined in Ref. [20]. They will be labeled as "CCGL operators" and can be found listed again in Appendix A for the convenience of the reader.

In the quark model, the matrix elements are obtained by explicit computation using the harmonic oscillator basis of eigenstates of H_0 with the help of (see e.g. Ref. [39])

$$\langle\gamma'j_1'j_2'JM|\vec{T}(k) \cdot \vec{U}(k)|\gamma j_1 j_2 JM\rangle$$
$$= (-)^{j_1+j_2'+J}\begin{Bmatrix} J & j_2' & j_1' \\ k & j_1 & j_2 \end{Bmatrix}$$
$$\times \sum_{\gamma''}\langle\gamma'j_1'||\vec{T}(k)||\gamma''j_1\rangle\langle\gamma''j_2'||\vec{U}(k)||\gamma j_2\rangle,$$

where $\langle\dots||\dots||\dots\rangle$ stands for the reduced matrix elements, the expression in brackets is a 6j-symbol and the dot in $\vec{T}(k) \cdot \vec{U}(k)$ means that all spatial indices of the tensor operators $\vec{T}(k)$ and $\vec{U}(k)$ of rank k are contracted. The reduced matrix elements of the spatial operator can be expressed in terms of radial integrals of the unknown functions $v_\varkappa^{0,1}$.

Our results for the matrix elements of the OGE + OME model $H = H_0 + V_{ss} + V_{so} + V_t$ in the quark model states basis are given in Table I, from where we can also read off the matrix elements of the more restricted OGE and OME models. The off-diagonal matrix elements are denoted as $^2N_J - {}^4N_J$.

The matrix elements shown in Table I involve m_0 and ten constants that are expressed in terms of the radial integrals I_2, I_4, U and J_4 of the unknown functions $v_\varkappa^{0,1}$ as

$$S^0 = -\frac{3}{2}\frac{\alpha^3}{\sqrt{\pi}}\left(I_2^0 + \frac{2}{3}\alpha^2 I_4^0\right), \qquad P_{2B}^0 = -4\frac{\alpha^5}{\sqrt{\pi}}U^0,$$

$$S'^0 = \frac{3}{2}\frac{\alpha^3}{\sqrt{\pi}}(I_2^0 - 2\alpha^2 I_4^0), \qquad P_{3B}^0 = \frac{8}{27}\frac{\alpha^5}{\sqrt{\pi}}U^0, \qquad D^0 = -\frac{2}{5}\frac{\alpha^5}{\sqrt{\pi}}J_4^0,$$

$$S^1 = \frac{3}{8}\frac{\alpha^3}{\sqrt{\pi}}(5I_2^1 - 2\alpha^2 I_4^1), \qquad P_{2B}^1 = 3\frac{\alpha^5}{\sqrt{\pi}}U^1, \qquad D^1 = \frac{3}{10}\frac{\alpha^5}{\sqrt{\pi}}J_4^1,$$

$$S'^1 = \frac{3}{8}\frac{\alpha^3}{\sqrt{\pi}}(I_2^1 - 2\alpha^2 I_4^1), \qquad P_{3B}^1 = -\frac{2}{27}\frac{\alpha^5}{\sqrt{\pi}}U^1, \qquad (18)$$

TABLE I. Matrix elements of the spin-spin V_{ss}, two-body spin-orbit V_{so-2B}, three-body spin-orbit V_{so-3B}, and tensor V_t component of the interaction. The 0 and 1 superscripts correspond to the OGE and OME case, respectively.

	H_0	V_{ss}^0	V_{ss}^1	$V_{so-2B}^{0,1}$	V_{so-3B}^0	V_{so-3B}^1	$V_t^{0,1}$
$^2N_{1/2}$	m_0	S^0	S^1	$2P_{2B}^{0,1}$	0	$-4P_{3B}^1$	0
$^4N_{1/2}$	m_0	$-S^0$	S'^1	$5P_{2B}^{0,1}$	0	0	$5D^{0,1}$
$^2N_{1/2} - {}^4N_{1/2}$	0	0	0	$P_{2B}^{0,1}$	P_{3B}^0	P_{3B}^1	$5D^{0,1}$
$^2N_{3/2}$	m_0	S^0	S^1	$-P_{2B}^{0,1}$	0	$2P_{3B}^1$	0
$^4N_{3/2}$	m_0	$-S^0$	S'^1	$2P_{2B}^{0,1}$	0	0	$-4D^{0,1}$
$^2N_{3/2} - {}^4N_{3/2}$	0	0	0	$\sqrt{\frac{5}{2}}P_{2B}^{0,1}$	$\sqrt{\frac{5}{2}}P_{3B}^0$	$\sqrt{\frac{5}{2}}P_{3B}^1$	$-\sqrt{\frac{5}{2}}D^{0,1}$
$^4N_{5/2}$	m_0	$-S^0$	S'^1	$-3P_{2B}^{0,1}$	0	0	$D^{0,1}$
$^2\Delta_{1/2}$	m_0	S'^0	S'^1	0	$-2P_{3B}^0$	$2P_{3B}^1$	0
$^2\Delta_{3/2}$	m_0	S'^0	S'^1	0	P_{3B}^0	$-P_{3B}^1$	0

where the radial integrals are

$$I_2^{0,1} = \int_0^\infty \rho^2 v_{ss}^{0,1}(\sqrt{2}\rho)e^{-\alpha^2\rho^2}d\rho,$$

$$J_4^{0,1} = \int_0^\infty \rho^4 v_t^{0,1}(\sqrt{2}\rho)e^{-\alpha^2\rho^2}d\rho,$$

$$I_4^{0,1} = \int_0^\infty \rho^4 v_{ss}^{0,1}(\sqrt{2}\rho)e^{-\alpha^2\rho^2}d\rho,$$

$$U^{0,1} = \int_0^\infty \rho^4 v_{so}^{0,1}(\sqrt{2}\rho)e^{-\alpha^2\rho^2}d\rho, \qquad (19)$$

and depend on the particular shapes and relative strengths of the spin-flavor interactions of a given model. These interactions will give the mass splittings within a spin-flavor multiplet.

The physical masses and mixing angles are obtained by diagonalizing the mass matrix, whose general form in the quark model basis of $S = 1/2$, $3/2$ quark spin states and its relation to the mixing angles can be found in Appendix B.

Notice that the tensor interaction and the two-body part of the spin-orbit interaction of the OGE and OME models are proportional to each other (i.e. $V_{so-2B}^1 \sim V_{so-2B}^0$ and $V_t^1 \sim V_t^0$). This allows us to list them in just one column in Table I, as they only differ in the numerical values of P_{2B}^1, P_{2B}^0 and D^1, D^0, respectively.

Alternatively, the mass matrix can also be written as a linear combination of the 18 spin-isospin CCGL operators [20]; see Appendix A. These operators were originally constructed to perform a $1/N_c$ expansion analysis, but they are also useful at fixed $N_c = 3$, since they provide an overcomplete basis for the mass matrix of the physical baryon states, that allows one to factor out explicitly the radial dependence of the states and interactions, as will be seen explicitly as a result of the matching to the quark model results. Grouping the effective $\ell = 0$, 1, 2 operators together we obtain the mass operator as

TABLE II.   General structure of the $\ell = 0$, 1 and 2 mass matrix expressed in terms of the CCGL operators that appear in the $1/N_c$ expansion.

	$O_{\ell=0}$	$O_{\ell=1}$	$O_{\ell=2}$
$^2N_{1/2}$	S_1	$-2P_1$	0
$^4N_{1/2}$	S_2	$5P_2$	$5D_1$
$^2N_{1/2} - {}^4N_{1/2}$	0	P_3	$-5D_2$
$^2N_{3/2}$	S_1	P_1	0
$^4N_{3/2}$	S_2	$2P_2$	$-4D_1$
$^2N_{3/2} - {}^4N_{3/2}$	0	$\sqrt{\frac{5}{2}}P_3$	$\sqrt{\frac{5}{2}}D_2$
$^4N_{5/2}$	S_2	$-3P_2$	D_1
$^2\Delta_{1/2}$	S_3	$-2P_4$	0
$^2\Delta_{3/2}$	S_3	P_4	0

$$M = \sum_{i=1}^{18} c_i O_i = O_{\ell=0} + O_{\ell=1} + O_{\ell=2}, \qquad (20)$$

where

$$O_{\ell=0} = \sum_{i=1,6,7,11,16} c_i O_i, \qquad (21)$$

$$O_{\ell=1} = \sum_{i=2,4,5,9,10,13,14,15} c_i O_i, \qquad (22)$$

$$O_{\ell=2} = \sum_{i=3,8,12,17,18} c_i O_i, \qquad (23)$$

and the operator coefficients c_i are numbers that are usually determined by fitting to data. We observe that the matrix elements of these operators, whose explicit expressions can be found in Ref. [20], have the general structure shown in Table II. For $\ell = 0$ they can be parametrized by three parameters $S_{1,2,3}$, for $\ell = 1$ they can be parametrized by four parameters $P_{1,2,3,4}$ and for $\ell = 2$ they can be parametrized by the two parameters $D_{1,2}$.

In Appendix C we give the linear relations satisfied by the operators on the nine-dimensional subspace of physical masses and mixing angles at $N_c = 3$, showing explicitly that there are only three, four and two independent operators (out of five, eight and five) for $\ell = 0$, 1, 2, respectively.

The relations between the coefficients c_i and the parameters S, P, D are given in Appendix D. Comparing Table II and Table I we find

$$S_1 = m_0 + S^0 + S^1, \qquad (24)$$

$$S_2 = m_0 - S^0 + S'^1, \qquad (25)$$

$$S_3 = m_0 + S'^0 + S'^1, \qquad (26)$$

$$P_1 = -P_{2B}^0 - P_{2B}^1 + 2P_{3B}^1, \qquad (27)$$

$$P_2 = P_{2B}^0 + P_{2B}^1, \qquad (28)$$

$$P_3 = P_{2B}^0 + P_{2B}^1 + P_{3B}^0 + P_{3B}^1, \qquad (29)$$

$$P_4 = P_{3B}^0 - P_{3B}^1, \qquad (30)$$

$$D_1 = D^0 + D^1, \qquad (31)$$

$$D_2 = -D^0 - D^1. \qquad (32)$$

This, together with Eqs. (D1)–(D9) and Eqs. (18)–(19), establishes the complete analytic matching of the generic quark model defined by Eqs. (13)–(16) to the spin-isospin effective operator expansion used in the $1/N_c$ studies of
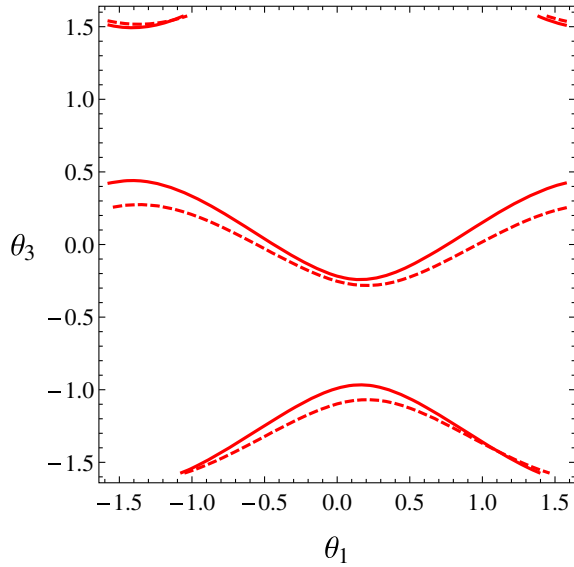
FIG. 1. The angle correlation implied by mass relation R1, Eq. (34), is shown as a full line. The dashed line corresponds to R1', Eq. (35), which differs from R1 by $1/N_c^2$ corrections.

excited baryons. Choosing $O_{1,...,9}$ as the basis of nine independent operators, we can solve $c_{1,...,9}$ in terms of the physical masses and mixing angles. The explicit expressions are given in Appendix E. A simple version of the quark model like the IK model provides a useful check of our expressions, as summarized in Appendix F.

For the OGE + OME model and the more restrictive OGE and OME model interactions there are constraints on these nine parameters leading to the parameter-free relations between the mixing angles and physical masses that will be discussed in the next section.

V. MASS-ANGLE RELATIONS

The general parametrization of the mass matrix shown in Table II involves nine parameters: three for the scalar part, four for the vector part and two for the tensor part of the interaction. These nine parameters can be solved in terms of the physical masses and mixing angles, which will allow us to study their variation on the mixing angles in Sec. VI.

However, for the most general OGE + OME quark model the 11 constants that give all the matrix elements in Table I only appear as seven independent combinations, as can be seen explicitly from Eqs. (24)–(32) and the

constraints given by Eq. (33) and Eq. (36) that will be discussed next. This implies that there must be two parameter-free relations among the masses and mixing angles.

The spin-orbit matrix elements of the OGE + OME model satisfy

$$P_1 + 2P_2 - P_3 + P_4 = 0, \tag{33}$$

implying our first mass-angle relation R1

$$\text{R1:}\ \frac{1}{2}(N_{1/2} - N'_{1/2})(3\cos 2\theta_1 + \sin 2\theta_1)$$
$$+ (N_{3/2} - N'_{3/2})\left(-\frac{3}{5}\cos 2\theta_3 + \sqrt{\frac{5}{2}}\sin 2\theta_3\right)$$
$$= -\frac{1}{2}(N_{1/2} + N'_{1/2}) + \frac{7}{5}(N_{3/2} + N'_{3/2})$$
$$- \frac{9}{5}N_{5/2} - 2\Delta_{1/2} + 2\Delta_{3/2}. \tag{34}$$

This relation was found for the first time in Ref. [29] [see Eq. (5) in this reference], where it was shown to hold for the most general quark model with two-body interactions. It was also pointed out that the same relation is obtained in the $1/N_c$ expansion by keeping all CCGL operators up to order $1/N_c$, using $N_c = 3$ to evaluate their matrix elements. The angle correlation it implies was already discussed in Fig. 5 of Ref. [40].

More recently R1 was found again in the form

$$\text{R1':}\ (N_{1/2} - N'_{1/2})(13\cos 2\theta_1 + 4\sqrt{2}\sin 2\theta_1)$$
$$- 4(N_{3/2} - N'_{3/2})(\cos 2\theta_3 - 2\sqrt{5}\sin 2\theta_3)$$
$$= -3(N_{1/2} + N'_{1/2}) + 12(N_{3/2} + N'_{3/2})$$
$$- 18N_{5/2} - 24\Delta_{1/2} + 24\Delta_{3/2}, \tag{35}$$

in Refs. [26,34] by expanding the matrix elements and dropping $1/N_c^2$ corrections in a $1/N_c$ analysis. Both relations R1 and R1' imply correlations among the mixing angles that are plotted in Fig. 1 using the experimental masses of Table III. Although the analytic expressions of R1 and R1' look very different, numerically the angle correlation that follows from them at $N_c = 3$ is very similar, a manifestation of the smallness of higher-order $1/N_c^2$ corrections.

TABLE III. The experimental values shown in the first line are taken from Ref. [41]. The mass spectra as obtained from the fits to the OGE and OME interactions, as discussed in Sec. VI, is shown in the last two lines. Masses are given in MeV.

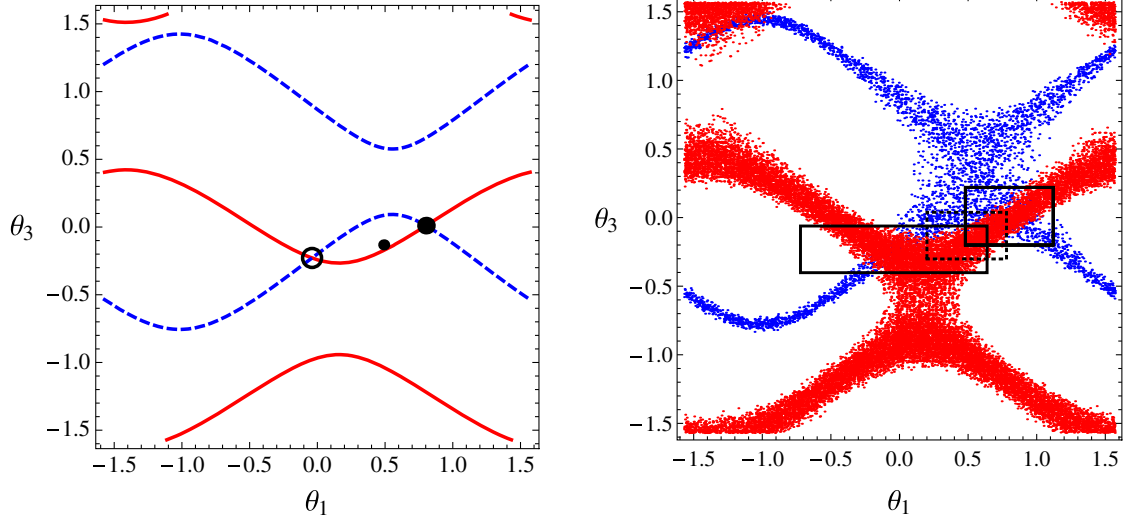|	$N_{1/2}(1535)$	$N'_{1/2}(1650)$	$N_{3/2}(1520)$	$N'_{3/2}(1700)$	$N_{5/2}(1675)$	$\Delta_{1/2}(1620)$	$\Delta_{3/2}(1700)$
PDG(2014)	1535 ± 10	1658 ± 13	1515 ± 5	1700 ± 50	1675 ± 5	1630 ± 30	1710 ± 40
OGE	1533 ± 37	1659 ± 43	1516 ± 36	1717 ± 19	1675 ± 16	1627 ± 39	1716 ± 30
OME	1535 ± 26	1659 ± 23	1515 ± 19	1693 ± 17	1675 ± 19	1637 ± 18	1683 ± 15

FIG. 2.   Angle correlations from the relations R1 and R2, given by Eq. (34) and Eq. (37). Left panel: The curves giving the $\theta_1 - \theta_3$ angle correlations intersect at sol–A $= (0.80, 0.01)$ (black dot) and sol–B $= (-0.04, -0.23)$ (circle), obtained using the central values of the masses. The smaller point in between corresponds to the best fit of the angles of Ref. [34]. Right panel: Scatter plot obtained including the experimental errors on the masses. The rectangles correspond to sol–A, sol–B and the best fit (dashed) with errors as in Table IV.

The second constraint in the OGE + OME case is

$$D_1 + D_2 = 0, \tag{36}$$

leading to the second mass-angle relation

R2: $5(N_{1/2} - N'_{1/2})(\cos 2\theta_1 + 2 \sin 2\theta_1)$

$$- 4(N_{3/2} - N'_{3/2})\left(2\cos 2\theta_3 + \sqrt{\frac{5}{2}} \sin 2\theta_3 \right)$$

$$= 5(N_{1/2} + N'_{1/2}) - 8(N_{3/2} + N'_{3/2}) + 6N_{5/2}. \tag{37}$$

The two OGE + OME relations R1 and R2 are plotted as the full and dashed curves in the left panel of Fig. 2 using the central values for the masses as given in Table III. Each relation gives different two-valued correlations between the two mixing angles (θ_1, θ_3). Their intersections give two possible solutions for the mixing angles, which we label as sol–A $= (0.80 \pm 0.32, 0.01 \pm 0.21)$, shown as a black dot, for the one with the larger value of θ_1 and sol–B $= (-0.04 \pm 0.68, -0.23 \pm 0.17)$, shown as a circle,

for the one with the smaller value of θ_1. The errors were obtained by propagating the errors of the experimental masses as given in Table III. The best values for the mixing angles obtained in Ref. [34] from a global fit to the masses and decays are $(0.49 \pm 0.29, -0.13 \pm 0.17)$, also shown in Fig. 2 as the smaller black dot.

When the uncertainties in the masses are taken into account the curves on the angles plane are expanded into bands, that are estimated in the scatter plot shown in the right panel. The rectangles correspond to sol–A, sol–B and the best-fit angles, with the error bars as in Table IV. In the upper left corner a third solution sol–C $\approx (-1.14, 1.50)$ is possible within the present experimental errors. It is similar to the $(-1.14, 1.40)$ solution $1'$ of the large-N_c analysis of Ref. [40], yet this solution is excluded by the best fit of Ref. [34] that also includes information on the decay properties of the baryons. We therefore do not consider sol–C any further here.

If we restrict the interactions to the OGE case we have one additional relation among matrix elements, namely

$$P_1 + P_2 = 0, \tag{38}$$

leading to

R3: $-25(N_{1/2} - N'_{1/2})\cos 2\theta_1 + 16(N_{3/2} - N'_{3/2})\cos 2\theta_3$

$$= 15(N_{1/2} + N'_{1/2}) - 24(N_{3/2} + N'_{3/2}) + 18N_{5/2}. \tag{39}$$

TABLE IV.   Mixing angles (in radians) for the two solutions (sol–A and sol–B) of the general OGE + OME interaction and for the OGE and OME model interactions.

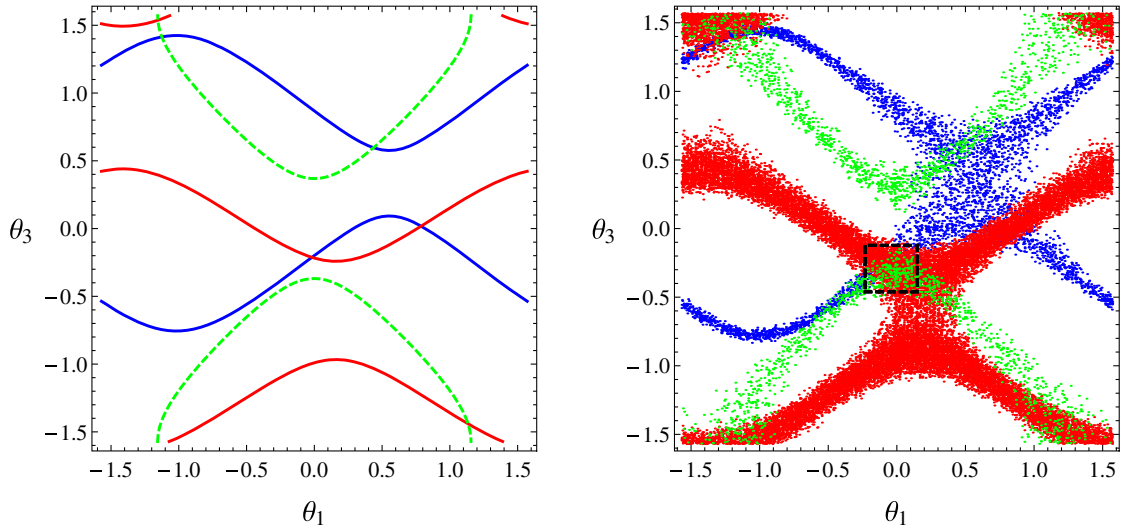|	sol–A	sol–B	OGE	OME
θ_1	0.80 ± 0.32	-0.04 ± 0.68	-0.04 ± 0.19	0.78 ± 0.28
θ_3	0.01 ± 0.21	-0.23 ± 0.17	-0.29 ± 0.17	0.11 ± 0.13

FIG. 3.   OGE mass-angle relation R3 [Eq. (39)] (dashed green) and general correlations R1 [Eq. (34)] (red) and R2 [Eq. (37)] (blue) Left: Using the central values of the masses. Right: Scatter plot obtained including the experimental errors on the masses and OGE angles with errors (dashed rectangle) as in Table IV.
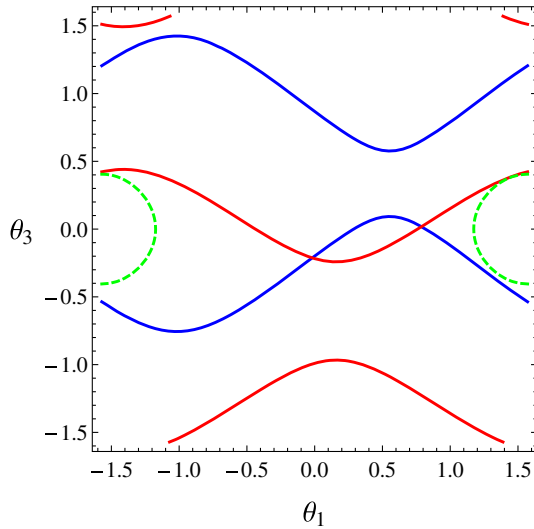
The relations R1, R2 and R3 that hold in the OGE case are shown in Fig. 3 next to the corresponding scatter plot. Taken together they exclude sol–A.

In the OME case, in addition to Eq. (33) and Eq. (36), we have two other constraints from the scalar and vector parts of the interaction

$$S_2 - S_3 = 0, \qquad (40)$$

$$P_1 + P_2 + 2P_4 = 0, \qquad (41)$$

giving the mass-angle relation

R4: $-(N_{1/2} - N'_{1/2})\cos 2\theta_1 - 2(N_{3/2} - N'_{3/2})\cos 2\theta_3$

$$= -(N_{1/2} + N'_{1/2}) - 2(N_{3/2} + N'_{3/2})$$

$$- 6N_{5/2} + 4\Delta_{1/2} + 8\Delta_{3/2}, \qquad (42)$$

and

R5: $-25(N_{1/2} - N'_{1/2})\cos 2\theta_1 + 16(N_{3/2} - N'_{3/2})\cos 2\theta_3$

$$= 15(N_{1/2} + N'_{1/2}) - 24(N_{3/2} + N'_{3/2})$$

$$+ 18N_{5/2} + 80\Delta_{1/2} - 80\Delta_{3/2}, \qquad (43)$$

respectively. In Fig. 4 we show R1, R2, R4 and R5 together with the corresponding scatter plot. It is important to stress
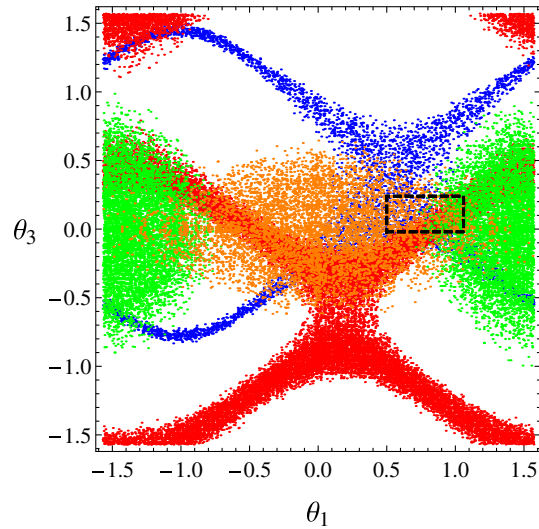

FIG. 4.   OME mass relations R4 [Eq. (42)] (orange) and R5 [Eq. (43)] (green), and general correlations R1 [Eq. (34)] (red) and R2 [Eq. (37)] (blue). Left: Using the central values of the masses R4 is not satisfied. Right: Scatter plot obtained including the experimental errors on the masses and OME angles with errors (dashed rectangle) as in Table IV.

TABLE V. Accuracy (in %) of the mass relations as defined in the text.

	(θ_1, θ_3)	R1	R2	R3	R4	R5
sol–A	(0.80, 0.01)	0.00	0.00	1.89	0.35	0.52
sol–B	(−0.04, −0.23)	0.00	0.00	0.17	0.15	1.08
sol–C	(−1.14, 1.50)	0.15	0.23	0.01	2.01	1.22

that R4 is not only predicted in the pure OME case, but also in the general OGE + OME interaction when the OGE part of the spin-spin interaction is a zero-range delta function. In that case $I_4^{0,1} = 0$ gives $S^0 = -S'^0$, which implies $S_2 = S_3$ and Eq. (40) holds for a generic OGE + OME interaction as well. The central orange area in the scatter plot of Fig. 4 corresponds to the region were R4 is satisfied within experimental errors and overlaps with the sol–A, sol–B and best-fit rectangles shown in Fig. 2, all compatible with a spin-spin interaction with a flavor-independent component of short range.

Finally, in order to quantify to what extent the relations R1…5 are satisfied, we define their accuracy (in %) as $100 \times |LHS - RHS|/(LHS + RHS)$ from the left-hand side (LHS) and right-hand side (RHS) of the equation $LHS = RHS$, corresponding to each of R1…5 written so that all terms in their LHS and RHS are positive. Taking typical values for the masses and splittings a good agreement is signaled by an accuracy value of less than 1%. Table V shows that R1 and R2 are always satisfied, the OGE relation R3 is favored by sol–B and sol–C, while the OME relations (R4 and R5) are favored by sol–A. R4 is well satisfied for both sol–A and sol–B, consistent with what was seen in the scatter plot. Again, this is compatible with a short range for the flavor-independent spin-spin component of the interaction.

VI. MIXING ANGLES AND BEST FITS

In this section we discuss the best fits to the mass matrix of the $L = 1$ excited baryons and the values we obtain for the mixing angles. We find that the two possible solutions for the angles of the general OGE + OME spin-flavor interaction are well approximated by the angles obtained in the more restrictive cases of an OGE or OME interaction.

For the general OGE+OME form of the quark-quark interaction, Eqs. (14)–(16), we obtain the two mass-angle

relations R1, R2, that follow from the two constraints, Eq. (33) and Eq. (36), leaving only seven parameters free, which are fitted to the seven masses and the two mixing angles obtained as sol–A and sol–B in the previous section. In the restricted model interactions, in addition to R1 and R2 we have more relations that follow from further constraints. In the OGE case we find one more relation, Eq. (38), leading to a six-parameter fit of the seven empirical masses. In the OME case there are two additional relations, Eqs. (40) and (41), leaving five parameters free for the fit. In both cases the corresponding mixing angles are obtained by diagonalizing the best-fit mass matrix. The errors in the mixing angles are obtained by error propagation using the expressions of Appendix B.

Before discussing the results of the fits, it is useful to redefine the parameters of the scalar part of the interaction as

$$S_1 = S_0 - \Delta S_{12},$$
$$S_2 = S_0 + \Delta S_{12},$$
$$S_3 = S_0 + \Delta S_3. \qquad (44)$$

In this way we can identify S_0 as the spin-independent contribution of the unit operator and separate it explicitly, as that contribution is at the much larger energy scale of the average mass of the multiplet and does not contribute to the mass splittings.

The results of the fits are summarized in Table VI, where the small numbers in italics indicate which parameters have not been fitted and were determined instead from the constraints that express them in terms of the free parameters. Within our minimal assumptions for the form of the quark-quark interactions, from the fits we obtain the typical sizes of 80, 30 and 10 MeV for the $\ell = 0$, 1, 2 components of the mass operator, respectively, with an average mass $S_0 \approx 1600$ MeV. The predictions for the OGE and OME mass spectra are included in Table III. Both model interactions are capable of perfectly fitting the data without any noticeable tension.

Our results for the mixing angles are summarized in Table IV and Fig. 5, where they are also compared with the best-fit angles of the global fit of Ref. [34], labeled here as GGS, that uses the $1/N_c$ hierarchy and also includes data on strong and electromagnetic decays. The two general

TABLE VI. The sol–A and sol–B fits of the general interaction have seven free parameters. The fits of the OGE and OME interactions have six and five parameters, respectively. The smaller numbers in italics indicate which parameters have not been fitted and were obtained instead from the constraints. All parameters are given in MeV.

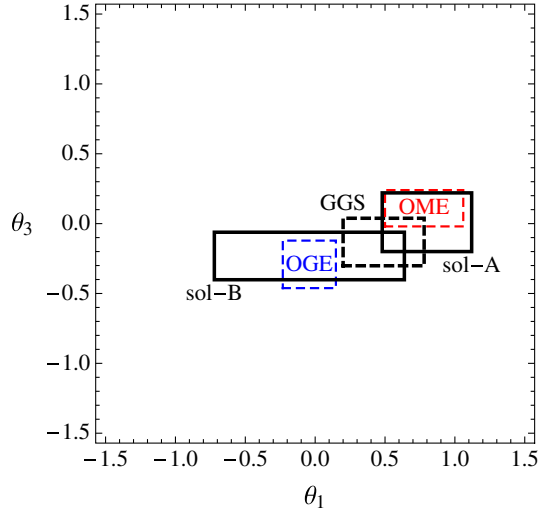|	S_0	ΔS_{12}	ΔS_3	P_1	P_2	P_3	P_4	D_1	D_2	$\chi^2_{\rm dof}$
sol–A	1606 ± 5	65 ± 11	77 ± 27	−28 ± 9	−5 ± 4	*−11 ± 18*	27 ± 14	−10 ± 3	*10 ± 3*	0.00
sol–B	1603 ± 9	75 ± 8	81 ± 28	−3.6 ± 5	−0.4 ± 3.2	*23 ± 14*	27 ± 12	−4 ± 6	*4 ± 6*	0.00
OGE	1607 ± 6	74 ± 9	80 ± 28	−0.4 ± 3	*0.4 ± 3*	*30 ± 17*	30 ± 14	−5 ± 4	*5 ± 4*	0.22
OME	1605 ± 4	63 ± 12	*63 ± 12*	*−26 ± 16*	−5 ± 4	*−20 ± 10*	15 ± 6	−8 ± 2	*8 ± 2*	0.53

FIG. 5. Mixing angles for sol–A, sol–B, the OME and OGE model interactions as in Table IV and the GGS best global fit values of Ref. [34].

solutions sol–A and sol–B can be associated to two different types of quark-quark interactions, labeled as OGE and OME. Within the present experimental uncertainties the global fit to the angles cannot distinguish among these two different possibilities.

The two solutions sol–A and sol–B differ in the details of their spin-orbit and tensor interactions. In Fig. 6 we show how the S, P, D parametrization of the mass matrix depends on the mixing angles. We include R1 (red curve), sol–A (black dot), sol–B (circle) and the GGS best fit (small black dot) in all contour plots, serving as reference points. Figure 6 shows that the S, P, D parameters are smooth functions of the angles, in contrast to the c_i operator coefficients of the $1/N_c$ studies that will be discussed in the next section. In particular, P_4 is independent of the mixing angles. In the left panel of Fig. 7 we show the $D_1 + D_2$ constraint, Eq. (36), which is a slowly varying function of the angles and is also approximately well satisfied by the best-fit values. In the right panel we plot $\sqrt{D_1^2 + D_2^2}$ to obtain a picture of the magnitude of the tensor interaction. We can see that sol–B is close to a region of small tensor interaction, while sol–A moves away from that region. In Fig. 8 we plot $\sqrt{P_1^2 + P_2^2 + P_3^2 + P_4^2}$ and we see that both sol–A and sol–B have spin-orbit matrix elements of similar strength.

From the fits (see Table VI) we observe that $\Delta S_{12} \approx \Delta S_3$ (i.e. $S_2 \approx S_3$), which is the telltale sign of a contact interaction in the flavor-independent spin-spin part, as discussed at the end of Sec. V and in Ref. [33]. This conclusion holds regardless of the spin-isospin structure of the interaction.

The values obtained for the fitted parameters can be understood qualitatively noting that there are some special mass combinations that are independent of the angles. We will discuss them next.

In the case of P_4 and ΔS_3, they are given by the splitting and the spin-averaged mass of the $\Delta_{3/2}, \Delta_{1/2}$ as follows:

$$P_4 = (\Delta_{3/2} - \Delta_{1/2})/3, \tag{45}$$

$$S_3 = (2\Delta_{3/2} + \Delta_{1/2})/3, \tag{46}$$

giving $P_4 \approx 27$ MeV, $\Delta S_3 = S_3 - S_0 \approx 78$ MeV using the empirical masses of Table III.

Taking the trace of the mass matrix for $J = 1/2$ and $J = 3/2$ we obtain the simple mass relation

$$N_{1/2} + N'_{1/2} = N_{3/2} + N'_{3/2}, \tag{47}$$

which is independent of the mixing angles and is observed to be well satisfied by the empirical masses as 3193 ± 16 MeV $= 3220 \pm 50$ MeV. It should therefore hold for all fits that accurately describe the spectrum, which for the matrix elements implies the constraint

$$3D_1 = P_1 - P_2. \tag{48}$$

This constraint is satisfied in different ways for the different fits we considered. In sol–B and the OGE fit both P_1 and P_2 are small, implying a small value of the tensor matrix element D_1. In sol–A and the OME fit P_2 is small, but P_1 is large, which gives a larger D_1 (see right panel of Fig. 7).

Another empirical relation that is well satisfied is

$$N_{5/2} = (2\Delta_{3/2} + \Delta_{1/2})/3, \tag{49}$$

as seen by inserting the empirical values for the masses: 1675 ± 5 MeV $= 1683 \pm 28$ MeV. For the matrix elements this implies

$$S_2 - S_3 = 3P_2 - D_1. \tag{50}$$

Using $S_2 = S_3$, which is satisfied within errors by all the fits, we get $D_1 = 3P_2$ as an approximate relation that explains the smallness of the spin-orbit matrix element P_2 as observed in all our fits correlating it with the typical size of the tensor matrix elements $D_{1,2}$.

VII. RELATION TO $1/N_c$ STUDIES

In this section we translate the constraints on matrix elements that we discussed in the previous sections to constraints on the coefficients c_i to gain further insight into their physical meaning, connecting in this way the QCD-based approach of the $1/N_c$ studies to a dynamical calculation in a quark model.

By choosing a basis of nine independent $1/N_c$ operators we can reexpress the matrix elements $S_{1,2,3}, P_{1,2,3,4}, D_{1,2}$ in terms of the operator coefficients $c_i(i = 1, 9)$. For the explicit relation between both parametrizations see Eqs. (D10)–(D18) in Appendix D. For the nine operator
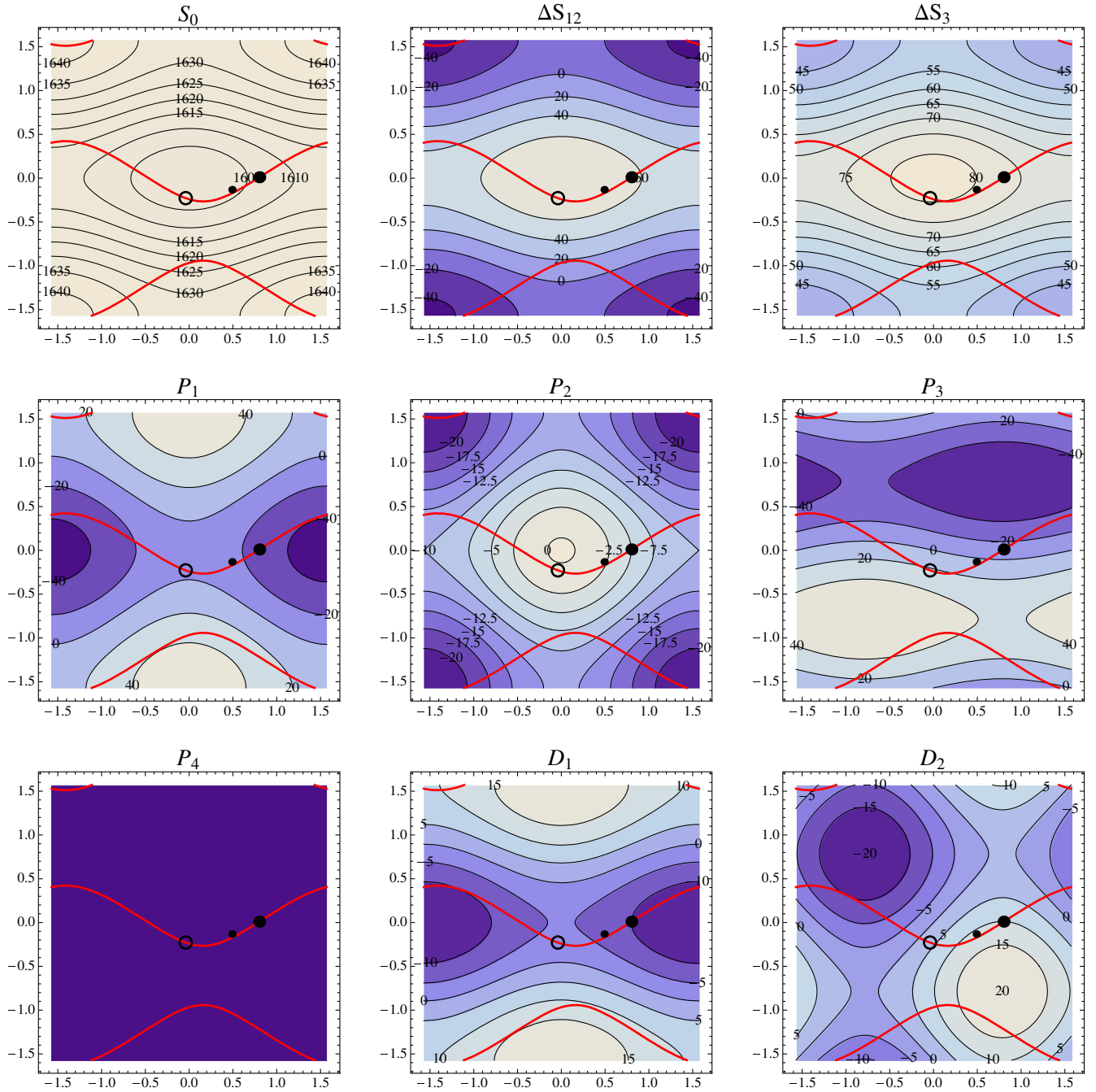
FIG. 6. Matrix elements as a function of the mixing angles (θ_1, θ_3). We also show the mixing angles for sol–A (black dot) and sol–B (circle). The smaller point in between corresponds to the GGS best-fit angles. The red curve shows the correlation between mixing angles given by relation R1 [Eq. (34)].

coefficients $c_{1...9}$ Fig. 9 gives the landscape on the mixing angles plane. We observe that all coefficients depend on the angles and c_3 and c_8 have the steepest slopes and are very sensitive to the mixing angle values, in contrast to the S, P, D parameters (see Fig. 6) where all the matrix elements were slowly varying functions of the angles θ_1, θ_3.

In Table VII we present the values we obtain for the coefficients c_i that correspond to the different cases we discussed: sol–A and sol–B for a general interaction

of OGE + OME type, and the restricted OGE and OME models. They are shown together with two recent determinations, from Refs. [26,34], labeled as FG and GGS respectively. The small numbers in italics indicate which coefficients have not been fitted and were determined instead from constraints that will be discussed below.

We will compare in the following with the values of the c_i in the last column of Table VII, obtained from the GGS
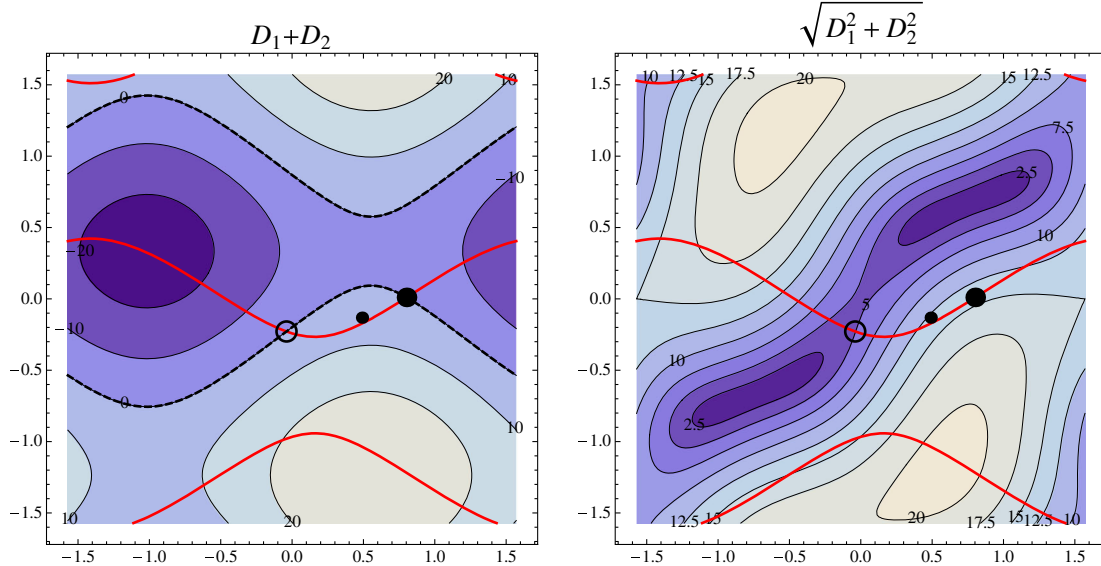
FIG. 7. The constraint $D_1 + D_2$ (dashed contour in left panel) and the magnitude of the tensor interaction $\sqrt{D_1^2 + D_2^2}$ (right panel) as a function of the mixing angles. R1, sol–A, sol–B and best fit value are as in Fig. 6.
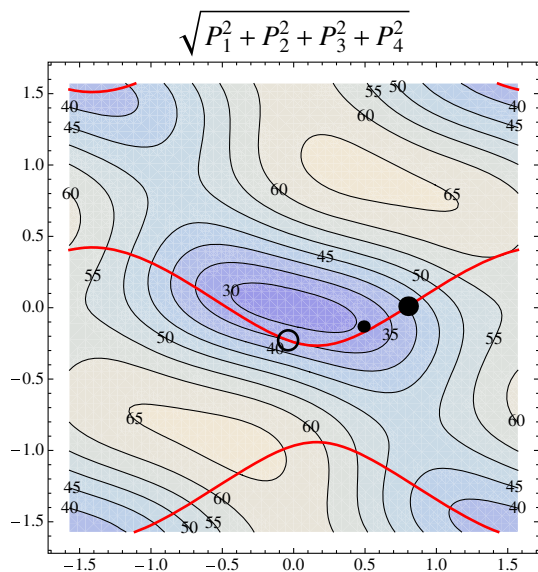

FIG. 8. The magnitude of the spin-orbit interaction $\sqrt{P_1^2 + P_2^2 + P_3^2 + P_4^2}$ as a function of the mixing angles. R1, sol–A, sol–B and best fit value are as in Fig. 6.

global fit of Ref. [34], where the hierarchy of $1/N_c$ operators was used, and the data on strong and electro-magnetic decays was also taken into account.

The first general relation, Eq. (33), corresponds to $c_9 = 0$ and is taken as a constraint in Refs. [26,34] as it corresponds to neglecting O_9, a higher-order operator in the $1/N_c$ expansion. The second general relation, Eq. (36), corresponds to $c_3 + 4c_8 = 0$. This evaluates to 104 ± 50 MeV $= 0$ for GGS, which at first sight seems to be violated badly. However, the relation to $D_1 + D_2$ is given

by Eq. (D8), which for the $O_{1\ldots9}$ basis evaluates to $c_3 + 4c_8 = 144(D_1 + D_2)$. The large numerical factor in this expression finally gives $D_1 + D_2 = 0.7 \pm 0.3$ MeV, which actually amounts to a small violation of the angle correlation imposed by $D_1 + D_2 = 0$, as $D_1 + D_2$ is a slowly varying function (see left panel of Fig. 7).

Restricting the general OGE + OME interaction to the OGE and OME model interactions we obtain from the OGE relation [Eq. (38)] the equivalent $c_4 = 0$ constraint, which is satisfied within errors as 38 ± 39 MeV $= 0$. The first of the OME relations, Eq. (40), implies $c_7 = 0$ which is satisfied as 4 ± 13 MeV $= 0$. The second OME relation, Eq. (41), implies $9c_4 = -12c_2 + 16c_5$ and is also satisfied as 342 ± 351 MeV $= 1232 \pm 639$ MeV.

We see that the general relations, as well as the more restricted OGE and OME relations are compatible with the GGS global fit values for the coefficients. This is consistent with what was observed for the mixing angles, as discussed in Sec. VI and summarized in Fig. 5.

If the general OGE + OME interaction with a contact interaction for the flavor-independent spin-spin part is considered, then $S_2 = S_3$ also implies $c_7 = 0$. This is well satisfied in all fits, giving a clear indication of a short-range interaction in the flavor-independent hyperfine part of the potential, one of the main conclusions of Ref. [33].

Finally we consider the constraints imposed by the two empirical relations, Eq. (47) and Eq. (49). The trace relation, Eq. (47) gives $3c_3 + 8c_5 = -12c_2 + 9c_4$ which is satisfied within errors and evaluates to 760 ± 322 MeV $= 642 \pm 427$ MeV. The $N_{5/2}$ relation, Eq. (49), gives $-3c_2 + \frac{1}{6}c_3 = 2c_5 + \frac{1}{3}c_8$ which is also satisfied within errors: 88 ± 60 MeV $= 119 \pm 74$ MeV. This is
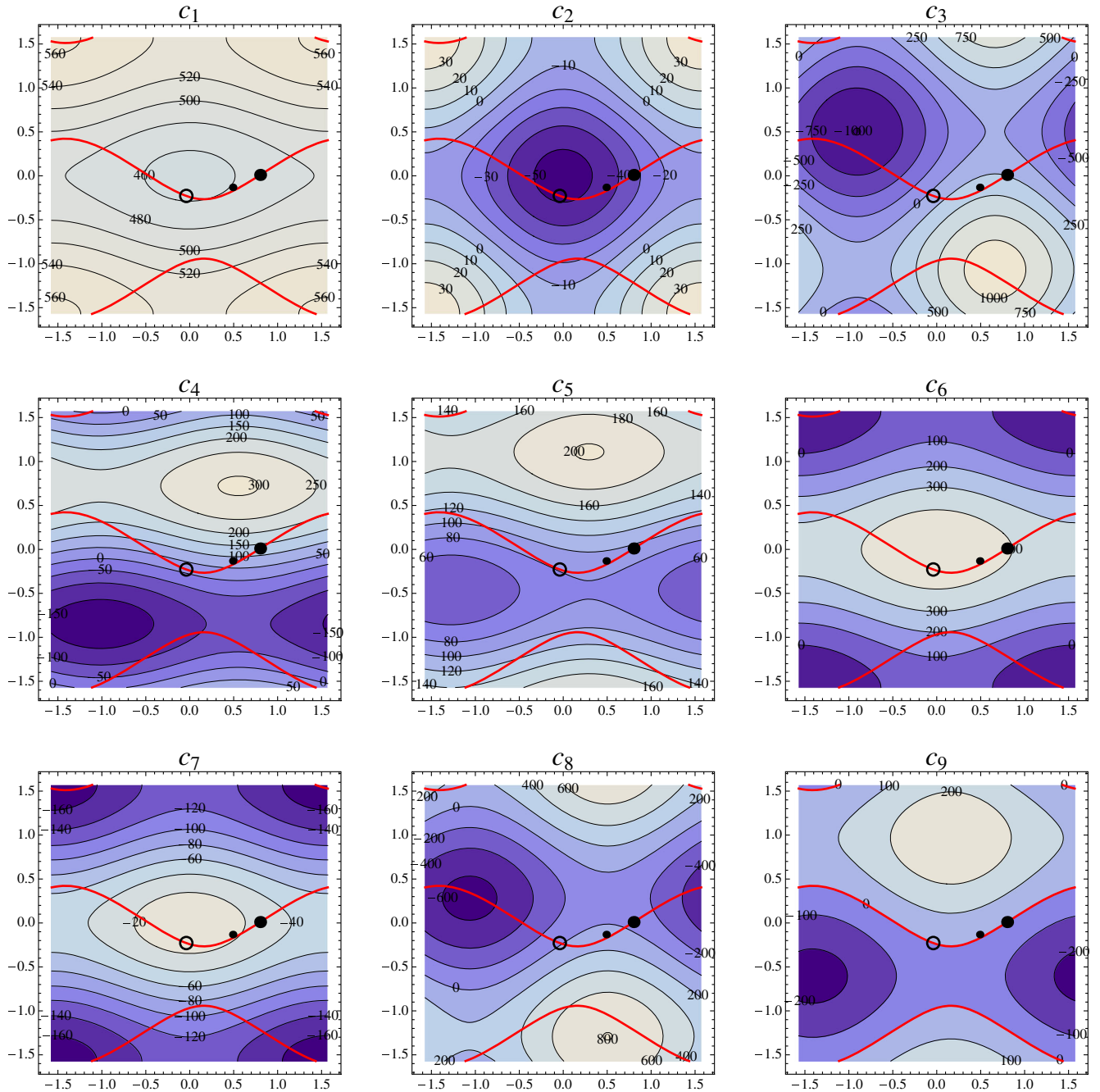
FIG. 9. Operator coefficients as a function of the mixing angles (θ_1, θ_3). We also show the mixing angles for sol–A (black dot) and sol–B (circle). The smaller point in between corresponds to the best-fit angles. The red curve shows the correlation between mixing angles given by relation R1 [Eq. (34)].

consistent with the good description of the spectrum obtained in the $1/N_c$ studies.

All these correlations among operator coefficients are not obvious when blindly performing a fit to the mass spectrum. The matching of a general quark model to the effective spin-flavor operators used in the $1/N_c$ expansion uncovers them and gives an insight into their dynamical meaning.

VIII. CONCLUSIONS

We showed that for a large class of nonrelativistic quark models, as defined by Eqs. (13)–(16), with flavor-dependent and flavor-independent quark-quark interactions, the observed mass spectrum of the nonstrange $L = 1$ excited baryons sets stringent constraints on the two mixing angles of the $J = 1/2, 3/2$ states. It is noteworthy that these

TABLE VII. Best fits for the operator coefficients (in MeV) and mixing angles (in radians). The last two columns show the results of Refs. [26,34], respectively. The smaller numbers in italics indicate which coefficients have not been fitted and were obtained from constraints.

	sol–A	sol–B	OGE	OME	FG	GGS
c_1	467 ± 10	458 ± 9	460 ± 9	472 ± 12	463 ± 2	497 ± 5
c_2	-33 ± 28	-52 ± 22	-61 ± 22	-10 ± 8	-36 ± 12	-24 ± 20
c_3	241 ± 76	85 ± 132	116 ± 104	200 ± 52	313 ± 69	96 ± 42
c_4	132 ± 48	16 ± 27	0	124 ± 41	65 ± 31	38 ± 39
c_5	95 ± 49	81 ± 42	88 ± 47	62 ± 29	71 ± 18	59 ± 37
c_6	408 ± 60	460 ± 50	456 ± 51	367 ± 75	443 ± 10	283 ± 36
c_7	-27 ± 64	-12 ± 65	-11 ± 65	0	-20 ± 31	4 ± 13
c_8	-60 ± 20	-21 ± 33	-29 ± 26	-50 ± 13	0	2 ± 7
c_9	0	0	0	0	0	0
θ_1	0.80 ± 0.32	-0.04 ± 0.68	-0.04 ± 0.19	0.78 ± 0.28	0.52 ± 0.13	0.49 ± 0.29
θ_3	0.01 ± 0.21	-0.23 ± 0.17	-0.29 ± 0.17	0.11 ± 0.13	-0.12 ± 0.09	-0.13 ± 0.17

constraints are independent of the detailed shape of the spin-spin, spin-orbit or tensor components of the effective quark-quark interaction. This is made manifest by expressing them as the solutions (sol–A and sol–B) of the two parameter-free relations R1 and R2 between empirical masses and mixing angles, shown in Eq. (34) and Eq. (37).

Restricting the form of the interactions to flavor-independent (OGE) or flavor-dependent (OME) terms only, we still obtained to a good approximation each of the two solutions we have in the most general case (OGE + OME). In the OGE case we obtained one additional correlation R3 [Eq. (39)], that is compatible with sol–B, while in the OME case we found two new parameter-free relations R4 and R5 [see Eqs. (42) and (43)], that are compatible with sol–A.

Only the first of the two OGE + OME relations (R1) was previously obtained in Ref. [29] by considering the most general two-body interactions. The angle correlation it implies was previously discussed in the $1/N_c$ analysis of Ref. [40] and more recently given in the form of R1' [Eq. (35)], by neglecting $1/N_c^2$ operators associated to three-body forces [26,34]. This relation alone is not sufficient to determine the angles from the mass spectrum without further constraints.

In Ref. [34] additional constraints from the $1/N_c$ expansion and the empirical data on decays were included in a global fit, resulting in the preferred GGS values for the mixing angles, which we used to compare with the constraints we obtained from the matching to a generic OGE + OME quark model. Within the present experimental errors we cannot exclude any of the two general solutions for the mixing angles, sol–A and sol–B, each of which can be well approximated by the restricted OME and OGE model interactions, respectively. This situation is summarized in Fig. 5.

We also discussed in detail the matching of the $1/N_c$ quark operator expansion to the nonrelativistic quark model, obtaining analytic expressions for all the operator coefficients in terms of integrals of the radial part of the

interactions, which are left unspecified in Eq. (19). The explicit relation between our parametrization of the mass matrix and the $1/N_c$ basis used in Refs. [26,34] is given by Eqs. (D10)–(D18) in Appendix D, establishing together with Eqs. (18), (19), and (24)–(32) the analytic correspondence with a large class of model interactions. It would be interesting to extend our matching calculation to the strong and electromagnetic decays of excited baryons, which we leave for future work.

Showing explicitly how the QCD-based $1/N_c$ analysis is related to a model calculation is useful to get an insight into the dynamics that generates the values of the fitted coefficients and mixing angles. It also uncovers correlations among the coefficients that are otherwise unnoticed when performing a fit and relates them to the attributes of the effective quark-quark interaction, as discussed in detail in Sec. V and Sec. VII.

We expect that the forthcoming results of lattice calculations, that will provide smaller errors in the mass spectrum and the possibility to explore the dependence of the baryon spectrum and the mixing angles as a function of the quark masses (see Ref. [26] for a pioneer effort in this direction), in combination with the $1/N_c$ expansion supplemented by a dynamical picture as provided here by matching to the quark model, will complement each other and constitute a solid toolbox for gaining further insight into the features of the nonperturbative regime of the strong interactions.

APPENDIX A: CCGL OPERATORS

Here we reproduce the list of 18 effective spin-flavor operators of Ref. [20]:

$$\mathcal{O}_1 = N_c \mathbb{1}, \tag{A1}$$

$$\mathcal{O}_2 = ls, \tag{A2}$$

$$\mathcal{O}_3 = \frac{1}{N_c} l^{(2)} g G_c, \tag{A3}$$

$$\mathcal{O}_4 = ls + \frac{4}{1 + N_c} lt G_c, \tag{A4}$$

$$\mathcal{O}_5 = \frac{1}{N_c} l S_c, \tag{A5}$$

$$\mathcal{O}_6 = \frac{1}{N_c} S_c^2, \tag{A6}$$

$$\mathcal{O}_7 = \frac{1}{N_c} s S_c, \tag{A7}$$

$$\mathcal{O}_8 = \frac{1}{N_c} l^{(2)} s S_c, \tag{A8}$$

$$\mathcal{O}_9 = \frac{N_c + 1}{N_c} \mathcal{O}_4 + \mathcal{O}_5 + \frac{8}{N_c^2} l^i g^{ja} \{S_c^j, G_c^{ia}\}, \tag{A9}$$

$$\mathcal{O}_{10} = \frac{1}{N_c} lg T_c, \tag{A10}$$

$$\mathcal{O}_{11} = \frac{1}{N_c} t T_c, \tag{A11}$$

$$\mathcal{O}_{12} = \frac{1}{N_c^2} l^{(2)} t \{S_c, G_c\}, \tag{A12}$$

$$\mathcal{O}_{13} = \frac{1}{N_c^2} (ls) S_c^2, \tag{A13}$$

$$\mathcal{O}_{14} = \frac{1}{N_c^2} \{l S_c, s S_c\}, \tag{A14}$$

$$\mathcal{O}_{15} = \frac{1}{N_c^2} (l S_c)(t T_c), \tag{A15}$$

$$\mathcal{O}_{16} = \frac{1}{N_c^2} g S_c T_c, \tag{A16}$$

$$\mathcal{O}_{17} = \frac{1}{N_c^2} l^{(2)} S_c S_c, \tag{A17}$$

$$\mathcal{O}_{18} = \frac{1}{N_c^2} l^{(2)} g S_c T_c. \tag{A18}$$

For $N_c = 3$ these 18 operators provide an overcomplete basis for the mass operator of nonstrange mixed-symmetric orbitally excited baryons.

APPENDIX B: GENERAL FORM OF THE 2×2 MASS MATRIX

We can write the mass matrix relevant for the $J = 1/2$ and $J = 3/2$ states in terms of the eigenvalues M_1 and M_2 and mixing angles as follows:

$$M = \begin{pmatrix} M_+ + M_- \cos 2\theta & M_- \sin 2\theta \\ M_- \sin 2\theta & M_+ - M_- \cos 2\theta \end{pmatrix}, \tag{B1}$$

with

$$M_+ = \frac{1}{2}(M_1 + M_2) = \frac{1}{2} \mathrm{Tr} M, \tag{B2}$$

$$M_- = \frac{1}{2}(M_1 - M_2) = \sqrt{\frac{1}{4}(\mathrm{Tr} M)^2 - \mathrm{Det} M}, \tag{B3}$$

where the mixing angles enter in the change of basis matrix C as

$$C = \begin{pmatrix} \cos \theta & \sin \theta \\ -\sin \theta & \cos \theta \end{pmatrix}, \qquad C^{-1} = \begin{pmatrix} \cos \theta & -\sin \theta \\ \sin \theta & \cos \theta \end{pmatrix}. \tag{B4}$$

We obtain the physical masses as

$$C.M.C^{-1} = \begin{pmatrix} M_1 & 0 \\ 0 & M_2 \end{pmatrix}. \tag{B5}$$

APPENDIX C: OPERATOR RELATIONS

Here we give the explicit form of the linear relations between CCGL operators that hold for arbitrary N_c on the nine-dimensional space spanned by the seven diagonal matrix elements and two off-diagonal matrix elements that are relevant for the physical states at $N_c = 3$.

$\ell = 0$:

$$\frac{N_c + 3}{2N_c^2(N_c - 1)} O_1 - \frac{1}{(N_c - 1)} O_6 + O_7 + O_{11} = 0, \tag{C1}$$

$$-\frac{N_c + 3}{2N_c^3(N_c - 1)} O_1 + \frac{N_c + 1}{2N_c(N_c - 1)} O_6 + O_{16} = 0. \tag{C2}$$

$\ell = 1$:

$$\frac{1}{2N_c} O_2 + \frac{N_c + 1}{4N_c} O_4 + \frac{1}{4} O_5 + O_{10} = 0, \tag{C3}$$

$$-\frac{2}{N_c^2}O_2 + \frac{N_c - 1}{4N_c^2}O_5 + \frac{N_c - 1}{4N_c}O_9 + O_{13} = 0, \quad \text{(C4)}$$

$$-\frac{4}{N_c^2}O_2 + \frac{3(N_c + 1)}{2N_c^2}O_4 + \frac{4N_c - 1}{2N_c^2}O_5 + \frac{2N_c - 1}{2N_c}O_9$$
$$+ O_{14} = 0, \quad \text{(C5)}$$

$$\frac{2}{N_c^2}O_2 - \frac{N_c + 1}{N_c^2}O_4 - \frac{N_c - 1}{2N_c^2}O_5 - \frac{N_c - 1}{2N_c}O_9 + O_{15} = 0.$$
$$\text{(C6)}$$

$\ell = 2$:

$$\frac{4}{N_c + 1}O_{12} + O_{17} = 0, \quad \text{(C7)}$$

$$-\frac{8}{N_c(N_c - 1)}O_3 - \frac{2}{N_c - 1}O_8 + O_{17} = 0, \quad \text{(C8)}$$

$$\frac{1}{N_c}O_8 + O_{18} = 0. \quad \text{(C9)}$$

APPENDIX D: RELATION BETWEEN OPERATOR COEFFICIENTS AND THE MATRIX ELEMENT PARAMETRIZATION

For $N_c = 3$ the coefficients in $O_{\ell=0,1,2}$ are related to their matrix elements given in Table II as follows.

$\ell = 0$:

$$c_1 - \frac{1}{6}c_{11} + \frac{1}{18}c_{16} = \frac{1}{3}(2S_1 - S_3), \quad \text{(D1)}$$

$$c_6 + \frac{1}{2}c_{11} - \frac{1}{3}c_{16} = -3S_1 + S_2 + 2S_3, \quad \text{(D2)}$$

$$c_7 - c_{11} = 2(S_2 - S_3). \quad \text{(D3)}$$

$\ell = 1$:

$$c_2 - \frac{1}{6}c_{10} + \frac{2}{9}c_{13} + \frac{4}{9}c_{14} - \frac{2}{9}c_{15} = -2(2P_2 + P_4),$$
$$\text{(D4)}$$

$$c_4 - \frac{1}{3}c_{10} - \frac{2}{3}c_{14} + \frac{4}{9}c_{15} = 4(P_2 - P_3 + P_4), \quad \text{(D5)}$$

$$c_5 - \frac{1}{4}c_{10} - \frac{1}{18}c_{13} - \frac{11}{18}c_{14} + \frac{1}{9}c_{15}$$
$$= P_1 - P_2 - P_3 + 4P_4, \quad \text{(D6)}$$

$$c_9 - \frac{1}{6}c_{13} - \frac{5}{6}c_{14} + \frac{1}{3}c_{15} = 3(P_1 + 2P_2 - P_3 + P_4).$$
$$\text{(D7)}$$

$\ell = 2$:

$$c_8 + \frac{1}{4}c_3 - \frac{1}{3}c_{18} - \frac{4}{3}c_{12} + \frac{4}{3}c_{17} = 36(D_1 + D_2), \quad \text{(D8)}$$

$$c_3 - \frac{4}{3}c_{12} + \frac{4}{3}c_{17} = 24(D_1 + 2D_2). \quad \text{(D9)}$$

Notice that the right-hand sides of Eq. (D7) and Eq. (D8) vanish for the OGE + OME model.

The operators O_1 to O_9 can be chosen as an independent basis for the physical states at $N_c = 3$. Setting $c_{10} = \cdots = c_{18} = 0$ we can express the coefficients $c_{1\ldots9}$ in terms of our mass matrix parametrization:

$$c_1 = \frac{1}{3}(2S_1 - S_3), \quad \text{(D10)}$$

$$c_2 = -2(2P_2 + P_4), \quad \text{(D11)}$$

$$c_3 = 24(D_1 + 2D_2), \quad \text{(D12)}$$

$$c_4 = 4(P_2 - P_3 + P_4), \quad \text{(D13)}$$

$$c_5 = P_1 - P_2 - P_3 + 4P_4, \quad \text{(D14)}$$

$$c_6 = -3S_1 + S_2 + 2S_3, \quad \text{(D15)}$$

$$c_7 = 2(S_2 - S_3), \quad \text{(D16)}$$

$$c_8 = 6(5D_1 + 4D_2), \quad \text{(D17)}$$

$$c_9 = 3(P_1 + 2P_2 - P_3 + P_4). \quad \text{(D18)}$$

Inverting the general relations given in Eqs. (D1)–(D9) we obtain

$$S_0 = 3c_1 + \frac{1}{2}c_6 - \frac{1}{4}c_{11}, \quad \text{(D19)}$$

$$S_1 = 3c_1 + \frac{1}{3}c_6 - \frac{1}{6}c_7 - \frac{1}{6}c_{11} + \frac{1}{18}c_{16}, \quad \text{(D20)}$$

$$S_2 = 3c_1 + \frac{2}{3}c_6 + \frac{1}{6}c_7 - \frac{1}{3}c_{11} - \frac{1}{18}c_{16}, \quad \text{(D21)}$$

$$S_3 = 3c_1 + \frac{2}{3}c_6 - \frac{1}{3}c_7 + \frac{1}{6}c_{11} - \frac{1}{18}c_{16}, \quad \text{(D22)}$$

$$P_1 = \frac{1}{6}c_2 - \frac{1}{4}c_4 + \frac{1}{9}c_5 + \frac{8}{27}c_9 + \frac{1}{36}c_{10} - \frac{1}{54}c_{13}$$
$$- \frac{2}{27}c_{14} - \frac{1}{27}c_{15}, \quad \text{(D23)}$$

$$P_2 = -\frac{1}{6}c_2 - \frac{1}{9}c_5 + \frac{1}{27}c_9 + \frac{1}{18}c_{10} - \frac{1}{27}c_{13}$$
$$- \frac{1}{27}c_{14} + \frac{1}{27}c_{15}, \quad \text{(D24)}$$

$$P_3 = -\frac{1}{3}c_2 - \frac{1}{4}c_4 + \frac{1}{9}c_5 - \frac{1}{27}c_9 + \frac{1}{9}c_{10} - \frac{2}{27}c_{13}$$
$$-\frac{1}{54}c_{14} - \frac{1}{27}c_{15}, \tag{D25}$$

$$P_4 = -\frac{1}{6}c_2 + \frac{2}{9}c_5 - \frac{2}{27}c_9 - \frac{1}{36}c_{10} - \frac{1}{27}c_{13}$$
$$-\frac{4}{27}c_{14} + \frac{1}{27}c_{15}, \tag{D26}$$

$$D_1 = -\frac{1}{36}c_3 + \frac{1}{18}c_8 - \frac{1}{27}c_{12} + \frac{1}{27}c_{17} - \frac{1}{54}c_{18}, \tag{D27}$$

$$D_2 = \frac{5}{144}c_3 - \frac{1}{36}c_8 - \frac{1}{108}c_{12} + \frac{1}{108}c_{17} + \frac{1}{108}c_{18}. \tag{D28}$$

It is convenient to remove the contribution of the unit operator to the spin-spin matrix elements by defining the parameters ΔS_{12}, ΔS_3; see Eq. (44). Here we obtain for them

$$\Delta S_{12} = \frac{1}{6}c_6 + \frac{1}{6}c_7 - \frac{1}{12}c_{11} - \frac{1}{18}c_{16}, \tag{D29}$$

$$\Delta S_3 = \frac{1}{6}c_6 - \frac{1}{3}c_7 + \frac{5}{12}c_{11} - \frac{1}{18}c_{16}. \tag{D30}$$

APPENDIX E: ANGLE DEPENDENCE OF THE OPERATOR COEFFICIENTS

With the choice of $\{O_1, ..., O_9\}$ as an independent basis we can solve $c_1 ... c_9$ in terms of the physical masses and mixing angles, obtaining

$$c_1 = \frac{1}{9}(N_{1/2} - N'_{1/2})\cos 2\theta_1 + \frac{2}{9}(N_{3/2} - N'_{3/2})\cos 2\theta_3 + \frac{1}{9}(N_{1/2} + N'_{1/2}) + \frac{2}{9}(N_{3/2} + N'_{3/2}) - \frac{1}{9}(\Delta_{1/2} + 2\Delta_{3/2}), \tag{E1}$$

$$c_2 = \frac{1}{6}(N_{1/2} - N'_{1/2})\cos 2\theta_1 + \frac{2}{15}(N_{3/2} - N'_{3/2})\cos 2\theta_3 - \frac{1}{6}(N_{1/2} + N'_{1/2}) - \frac{2}{15}(N_{3/2} + N'_{3/2}) + \frac{3}{5}N_{5/2} + \frac{2}{3}(\Delta_{1/2} - \Delta_{3/2}), \tag{E2}$$

$$c_3 = (N'_{1/2} - N_{1/2})(\cos 2\theta_1 + 4\sin 2\theta_1) - (N'_{3/2} - N_{3/2})\left(\frac{8}{5}\cos 2\theta_3 + 4\sqrt{\frac{2}{5}}\sin 2\theta_3\right) + N'_{1/2} + N_{1/2} - \frac{8}{5}(N'_{3/2} + N_{3/2}) + \frac{6}{5}N_{5/2}, \tag{E3}$$

$$c_4 = -\frac{1}{6}(N_{1/2} - N'_{1/2})(\cos 2\theta_1 + 2\sin 2\theta_1) - (N_{3/2} - N'_{3/2})\left(\frac{2}{15}\cos 2\theta_3 + \frac{5}{3}\sqrt{\frac{2}{5}}\sin 2\theta_3\right) + \frac{1}{6}(N_{1/2} + N'_{1/2})$$
$$+ \frac{2}{15}(N_{3/2} + N'_{3/2}) - \frac{3}{5}N_{5/2} - \frac{4}{3}(\Delta_{1/2} - \Delta_{3/2}), \tag{E4}$$

$$c_5 = -\frac{1}{4}(N_{1/2} - N'_{1/2})\left(\frac{1}{2}\cos 2\theta_1 + \frac{1}{3}\sin 2\theta_1\right) + (N_{3/2} - N'_{3/2})\left(\frac{1}{5}\cos 2\theta_3 - \frac{1}{6}\sqrt{\frac{5}{2}}\sin 2\theta_3\right) - \frac{5}{24}(N_{1/2} + N'_{1/2})$$
$$+ \frac{2}{15}(N_{3/2} + N'_{3/2}) + \frac{3}{20}N_{5/2} - \frac{4}{3}(\Delta_{1/2} - \Delta_{3/2}), \tag{E5}$$

$$c_6 = -\frac{7}{12}(N_{1/2} - N'_{1/2})\cos 2\theta_1 - \frac{7}{6}(N_{3/2} - N'_{3/2})\cos 2\theta_3 - \frac{5}{12}(N_{1/2} + N'_{1/2}) - \frac{5}{6}(N_{3/2} + N'_{3/2}) + \frac{1}{2}N_{5/2}$$
$$+ \frac{2}{3}(\Delta_{1/2} + 2\Delta_{3/2}), \tag{E6}$$

$$c_7 = -\frac{1}{6}(N_{1/2} - N'_{1/2})\cos 2\theta_1 - \frac{1}{3}(N_{3/2} - N'_{3/2})\cos 2\theta_3 + \frac{1}{6}(N_{1/2} + N'_{1/2}) + \frac{1}{3}(N_{3/2} + N'_{3/2}) + N_{5/2} - \frac{2}{3}(\Delta_{1/2} + 2\Delta_{3/2}), \tag{E7}$$

$$c_8 = -(N_{1/2} - N'_{1/2})\left(\frac{5}{4}\cos 2\theta_1 + 2\sin 2\theta_1\right)$$

$$+ 2(N_{3/2} - N'_{3/2})\left(\cos 2\theta_3 + \sqrt{\frac{2}{5}}\sin 2\theta_3\right)$$

$$+ \frac{5}{4}(N_{1/2} + N'_{1/2}) - 2(N_{3/2} + N'_{3/2}) + \frac{3}{2}N_{5/2},$$

$$\text{(E8)}$$

$$c_9 = -\frac{1}{4}(N_{1/2} - N'_{1/2})(3\cos 2\theta_1 + \sin 2\theta_1)$$

$$+ \frac{1}{2}(N_{3/2} - N'_{3/2})\left(\frac{3}{5}\cos 2\theta_3 - \sqrt{\frac{5}{2}}\sin 2\theta_3\right)$$

$$+ \frac{7}{10}(N_{3/2} + N'_{3/2}) - \frac{1}{4}(N_{1/2} + N'_{1/2})$$

$$- \frac{9}{10}N_{5/2} - \Delta_{1/2} + \Delta_{3/2}. \quad \text{(E9)}$$

APPENDIX F: MASS OPERATOR, MIXING ANGLES AND OPERATOR EXPANSION MATCHING FOR THE ISGUR-KARL MODEL

The Isgur-Karl model [31] is defined by the quark Hamiltonian

$$\mathcal{H}_{\text{IK}} = H_0 + \mathcal{H}_{\text{hyp}}, \quad \text{(F1)}$$

where H_0 contains the confining potential and kinetic terms of the quark fields, and is symmetric under spin and isospin. The hyperfine interaction $\mathcal{H}_{\text{hyp}}$ is given by

$$\mathcal{H}_{\text{hyp}} = A \sum_{i<j} \left[\frac{8\pi}{3} \vec{s}_i \cdot \vec{s}_j \delta^{(3)}(\vec{r}_{ij}) \right.$$

$$\left. + \frac{1}{r_{ij}^3}(3\vec{s}_i \cdot \hat{r}_{ij}\vec{s}_j \cdot \hat{r}_{ij} - \vec{s}_i \cdot \vec{s}_j) \right], \quad \text{(F2)}$$

where A determines the strength of the interaction [42], and $\vec{r}_{ij} = \vec{r}_i - \vec{r}_j$ is the distance between quarks i, j. The first term is a contact spin-spin interaction, and the second describes a tensor interaction between two dipoles. Both terms are flavor independent. This interaction Hamiltonian is an approximation to the gluon-exchange interaction, neglecting the spin-orbit terms. The entire spectroscopy of the $L = 1$ baryons is fixed by one single constant δ, defined as

$\delta = A\frac{2\alpha^3}{\sqrt{2\pi}} \simeq 300$ MeV, along with an overall additive constant m_0, the average mass for the multiplet $m_0 \simeq 1610$ MeV, and the model is very predictive. The explicit mass matrix is given by

$$M_{1/2} = m_0 + \frac{1}{4}\delta\begin{pmatrix} -1 & -1 \\ -1 & 0 \end{pmatrix}, \quad \text{(F3)}$$

$$M_{3/2} = m_0 + \frac{1}{4}\delta\begin{pmatrix} -1 & \frac{1}{\sqrt{10}} \\ \frac{1}{\sqrt{10}} & \frac{9}{5} \end{pmatrix}, \quad \text{(F4)}$$

$$M_{5/2} = m_0 + \frac{1}{5}\delta, \quad \text{(F5)}$$

$$\Delta_{1/2} = \Delta_{3/2} = m_0 + \frac{1}{4}\delta. \quad \text{(F6)}$$

The mixing angles are independent of the hadron masses, and are given by

$$\theta_1^{\text{IK}} = \arctan\left(\frac{1}{2}(\sqrt{5} - 1)\right) = 0.55,$$

$$\theta_3^{\text{IK}} = \arctan\left(-\frac{\sqrt{10}}{14 + \sqrt{206}}\right) = -0.11. \quad \text{(F7)}$$

The matching performed in Ref. [30] to the $1/N_c$ operators obtained $c_1 = \frac{1}{3}m_0 - \frac{1}{4}\delta = 462$ MeV, $c_6 = \frac{3}{2}\delta = 450$ MeV, $c_8 = -\frac{6}{5}\delta = -360$ MeV, and $c_{17} = \frac{9}{10}\delta = 270$ MeV, with all the other coefficients being zero. The corresponding $\chi^2 = 33$ is large because, due to the absence of spin-orbit forces, the IK model fails to describe the splitting of the $\Delta_{1/2}(1620)$ and $\Delta_{3/2}(1700)$, and the mass of the $N_{1/2}(1535)$ comes out too low. This explains why the $(\theta_1^{\text{IK}}, \theta_3^{\text{IK}})$ fall outside the OGE rectangle of our Fig. 3, which was obtained from a fit with a much smaller value of χ^2.

Evaluating the radial integrals, Eq. (19), we obtain for our matrix element parametrization $S_1 = m_0 - \frac{1}{4}\delta = 1535$ MeV, $S_2 = S_3 = m_0 + \frac{1}{4}\delta = 1685$ MeV, $P_1 = P_2 = P_3 = P_4 = 0$, $D_1 = -D_2 = -\frac{1}{20}\delta = -15$ MeV. In terms of the redefined spin-spin parameters [see Eq. (44)], $S_0 = m_0 = 1610$ MeV, $\Delta S_{12} = \Delta S_3 = \frac{1}{4}\delta = 75$ MeV. In this way the IK model provides a simple analytical check of our general expressions.

[1] R. G. Edwards, J. J. Dudek, D. G. Richards, and S. J. Wallace, Phys. Rev. D **84**, 074508 (2011).

[2] R. G. Edwards, N. Mathur, D. G. Richards, and S. J. Wallace (Hadron Spectrum Collaboration), Phys. Rev. D **87**, 054506 (2013).

[3] S. Capstick and W. Roberts, Prog. Part. Nucl. Phys. **45**, S241 (2000).

[4] E. Klempt and J. M. Richard, Rev. Mod. Phys. **82**, 1095 (2010).

[5] V. Crede and W. Roberts, Rep. Prog. Phys. **76**, 076301 (2013).

[6] G.'t Hooft, Nucl. Phys. **B72**, 461 (1974).

[7] E. Witten, Nucl. Phys. **B160**, 57 (1979).

[8] J. L. Gervais and B. Sakita, Phys. Rev. Lett. **52**, 87 (1984).

[9] J. L. Gervais and B. Sakita, Phys. Rev. D **30**, 1795 (1984).

[10] K. Bardakci, Nucl. Phys. **B243**, 197 (1984).

[11] R. F. Dashen and A. V. Manohar, Phys. Lett. B **315**, 425 (1993).

[12] E. E. Jenkins, Phys. Lett. B **315**, 441 (1993).

[13] R. F. Dashen, E. E. Jenkins, and A. V. Manohar, Phys. Rev. D **49**, 4713 (1994); **51**, 2489(E) (1995).

[14] C. Carone, H. Georgi, and S. Osofsky, Phys. Lett. B **322**, 227 (1994).

[15] M. A. Luty and J. March-Russell, Nucl. Phys. **B426**, 71 (1994).

[16] R. F. Dashen, E. E. Jenkins, and A. V. Manohar, Phys. Rev. D **51**, 3697 (1995).

[17] J. L. Goity, Phys. Lett. B **414**, 140 (1997).

[18] D. Pirjol and T. M. Yan, Phys. Rev. D **57**, 1449 (1998).

[19] D. Pirjol and T. M. Yan, Phys. Rev. D **57**, 5434 (1998).

[20] C. E. Carlson, C. D. Carone, J. L. Goity, and R. F. Lebed, Phys. Rev. D **59**, 114008 (1999).

[21] C. L. Schat, J. L. Goity, and N. N. Scoccola, Phys. Rev. Lett. **88**, 102002 (2002).

[22] J. L. Goity, C. L. Schat, and N. N. Scoccola, Phys. Rev. D **66**, 114014 (2002).

[23] N. Matagne and F. Stancu, Rev. Mod. Phys. **87**, 211 (2015).

[24] E. E. Jenkins, A. V. Manohar, J. W. Negele, and A. Walker-Loud, Phys. Rev. D **81**, 014502 (2010).

[25] A. C. Cordón, T. DeGrand, and J. L. Goity, Phys. Rev. D **90**, 014505 (2014).

[26] I. P. Fernando and J. L. Goity, Phys. Rev. D **91**, 036005 (2015).

[27] D. Pirjol and C. Schat, Phys. Rev. D **78**, 034026 (2008).

[28] H. Collins and H. Georgi, Phys. Rev. D **59**, 094010 (1999).

[29] D. Pirjol and C. Schat, Phys. Rev. Lett. **102**, 152002 (2009).

[30] L. Galeta, D. Pirjol, and C. Schat, Phys. Rev. D **80**, 116004 (2009).

[31] N. Isgur and G. Karl, Phys. Lett. B **72**, 109 (1977).

[32] N. Isgur and G. Karl, Phys. Rev. D **18**, 4187 (1978).

[33] D. Pirjol and C. Schat, Phys. Rev. D **82**, 114005 (2010).

[34] E. G. de Urreta, J. L. Goity, and N. N. Scoccola, Phys. Rev. D **89**, 034024 (2014).

[35] Notice the change of notation respect to Ref. [20] regarding the meaning of the prime on states. Instead of $S = 3/2$ quark model states, N'_J are now physical states.

[36] A. De Rujula, H. Georgi, and S. L. Glashow, Phys. Rev. D **12**, 147 (1975).

[37] A. Manohar and H. Georgi, Nucl. Phys. **B234**, 189 (1984).

[38] L. Y. Glozman and D. O. Riska, Phys. Rep. **268**, 263 (1996).

[39] A. R. Edmonds, *Angular Momentum in Quantum Mechanics* (Princeton University, Princeton, NJ, 1974).

[40] D. Pirjol and C. Schat, Phys. Rev. D **67**, 096009 (2003).

[41] K. A. Olive *et al.* (Particle Data Group Collaboration), Chin. Phys. C **38**, 090001 (2014).

[42] In Ref. [31] A is taken as $A = \frac{2\alpha_S}{3m^2}$.